Letter | Editors' Suggestion

Fully thermal meta-GGA exchange correlation free-energy density functional

Katerina P. Hilleke [1,*] Valentin V. Karasiev [1,†] S. B. Trickey [2] R. M. N. Goshadze [1] and S. X. Hu [1,3,4]

[1]*Laboratory for Laser Energetics, University of Rochester, 250 East River Road, Rochester, New York 14623, USA*

[2]*Quantum Theory Project, Departments of Physics and of Chemistry, University of Florida, Gainesville, Florida 32611, USA*

[3]*Department of Physics and Astronomy, University of Rochester, Rochester, New York 14623, USA*

[4]*Department of Mechanical Engineering, University of Rochester, Rochester, New York 14623, USA*

(Received 17 January 2025; accepted 2 May 2025; published 27 May 2025)

The application of density functional theory to materials in the warm dense matter regime has motivated the development of exchange-correlation functionals which incorporate proper, explicit temperature dependence. Previous work has yielded fully thermal exchange-correlation free energy functionals at the local density approximation and generalized gradient approximation (GGA) levels of refinement. Recently, an additive thermal correction scheme was utilized to construct a meta-GGA exchange-correlation (XC) functional in which thermal effects are treated at the GGA level. The *f*TSCAN free-energy XC functional presented here includes thermal effects through the meta-GGA level in the context of the SCAN (strongly constrained and appropriately normed) ground-state functional. The *f*TSCAN functional provides generality while achieving similar performance to a thermal GGA functional at high temperatures, e.g., pressures within 1% of path integral Monte Carlo simulations of warm dense hydrogen and a significant improvement over ground-state functionals. At low temperatures, *f*TSCAN demonstrates improvements in accuracy relative to lower-level and deorbitalized functionals, indicating that calculations using *f*TSCAN may be expected to perform well across experimentally relevant densities and pressures.

DOI: 10.1103/PhysRevMaterials.9.L050801

Introduction. Density functional theory (DFT) [1] has become the computational workhorse for electronic structure calculations, being a routine part of studies, especially in materials science and quantum chemistry. In the Kohn-Sham formalism [2], the sole approximation is in the exchange-correlation (XC) functional. It is no great surprise, then, that substantial effort has been devoted to improving and testing various approximate XC functionals. The surprising success of the earliest and simplest of these, the local density approximation (LDA), can be traced to its satisfaction of certain exact constraints on the true XC functional [3,4]. Construction of more refined (so-called higher level) XC functionals with added ingredients—the generalized gradient approximation (GGA), with added dependence on the density gradient, and meta-GGAs with added dependence on the kinetic energy density—frequently has followed constraint-based development schemes [5–8].

What might be missed in the face of the staggering array of XC functionals in the literature is the fact that nearly all were developed under the assumption that the electronic temperature $T \approx 0$ K. That is reasonable enough for most traditional applications in materials science and quantum chemistry, but over the past decade DFT has become a widely used tool for accurate simulations of warm dense matter (WDM). That broad, complicated regime bridges condensed matter and plasmas. It occurs within giant planet and stellar interiors as well as along the path to inertial confinement fusion [9–11]. Typical maximum pressures surpass 1 Mbar and electron temperatures range from roughly 1 to 100 eV. Under such conditions, explicit thermal XC effects cannot be neglected. Formally, this is done with Mermin's free-energy extension of Kohn-Sham DFT, denoted hereafter as MKS [12]. From a practitioner's point of view, the use of XC functionals with explicit temperature dependence improves the agreement between DFT simulations and experimental observations [13–15]. Indeed, even a lower-level XC functional with proper inclusion of thermal effects has been shown to outperform a higher-level ground-state XC functional when applied to warm dense matter [16].

Much as ground-state XC functional development relied at first on accurate parametrization of the exact XC energy of the homogeneous electron gas (HEG), thermal XC functional development starts at the LDA level from parametrization of the XC *free* energy per particle $f_{\rm xc}$ computed from quantum Monte Carlo results [17,18]. Those parametrizations give rise to the LDA-level XC free energy functionals (corr)KSDT [19,20] and GDSMFB [21]. At the GGA level, the KDT16 free-energy density functional incorporates density-gradient thermal effects via temperature-dependent reduced density gradient variables derived from the finite-T XC free-energy gradient expansion [20]. Additive [22] and multiplicative [23] thermal correction schemes, by which a ground-state GGA functional is augmented with a LDA-level thermal correction factor, have been developed as well. An additive GGA-level correction also was applied to a ground-state meta-GGA-level functional [14]. To date, however, to the best of our

*Contact author: khil@lle.rochester.edu

†Contact author: vkarasev@lle.rochester.edu

knowledge, no XC functional which incorporates thermal XC effects fully at the meta-GGA level has been published.

Here we describe such a functional, denoted *f*TSCAN, an extension of the strongly constrained and appropriately normed (SCAN) functional [5] to finite temperature conditions. SCAN obeys all 17 known exact constraints achievable at the ground state meta-GGA level and has demonstrated high accuracy across a broad range of materials [5,24,25]. It is extremely desirable for a functional to exhibit such breadth of accuracy, for example, in the construction of wide-ranging multiphase equation of state (EOS) tables.

To build *f*TSCAN, we generalize the ground-state input variables—reduced density gradients and kinetic energy densities—to account properly for constraints on finite-temperature behavior and limits. The resulting functional is well-equipped to handle explicit thermal effects in the inhomogeneous electron densities of real systems. We test the performance of *f*TSCAN with model systems chosen to highlight differences between free-energy and ground-state functionals at the LDA, GGA, and meta-GGA levels and compare the performance of *f*TSCAN in *ab initio* molecular dynamics (AIMD) simulations with other thermal functionals. Finally, we confirm that the formidable accuracy of ground-state SCAN is unaffected in the low-temperature limit, positioning *f*TSCAN as an excellent choice for use from ambient conditions to and through the WDM regime.

Systematic incorporation of thermal XC effects. At the meta-GGA level, in addition to the electron density and its gradient, ground state XC functionals take as input the orbital kinetic energy density (KED) $t_s = \frac{1}{2}\sum_{i=1}^{N_e} |\nabla\psi_i|^2$ of N_e electrons in the ground state. Typically, t_s is combined with the von Weizsäcker (t_{vW}) and Thomas-Fermi (t_{TF}) kinetic energy densities into some dimensionless parameter, usually called an isoorbital indicator. Such indicators are built to distinguish orbital overlap types ranging from single-orbital-like to metallic [26,27]. For SCAN, the only isoorbital indicator is $\alpha(n, \nabla n, \{\psi\}) := (t_s - t_{vW})/t_{TF}$. Exchange and correlation energies are interpolated between $\alpha = 0$ (single-orbital-like) and $\alpha = 1$ (metallic) cases combined with extrapolation to $\alpha \to \infty$ (weakly covalent).

For a fully thermal meta-GGA XC functional, proper T dependence must be incorporated into α through T-dependent KEDs. An important hint for this procedure is recognition that the numerator of α corresponds to the Pauli KED, $t_\theta := t_s - t_{vW}$. At $T = 0$ K, it is known that $t_{vW}[n] \leqslant t_s[n]$ as shown in Ref. [28], hence straightforwardly one has $\alpha \geqslant 0$. The finite-T analog of the Pauli KED, τ_θ, also has been proven to be strictly positive [29,30]. Under these conditions, $\tau_\theta = \tau_s^{MKS} - t_{vW}$ uses the finite-T KED τ_s^{MKS} (defined below) and the ground-state von Weizsäcker KED form. Then the T-dependent isoorbital indicator α_T becomes

$$\alpha_T(n, \nabla n, \{\psi\}, T) = \frac{\tau_s^{MKS}(\{\psi\}, T) - t_{vW}(n, \nabla n)}{\tau_{TF}(n, T)}. \quad (1)$$

In what follows, we simplify notation to $\alpha_T(n, \nabla n, \{\psi\})$ or simply α_T to remind the reader of the explicit T dependence. The T-dependent orbital kinetic energy is already well understood according to Mermin's work [12] via Fermi-Dirac occupations $f_i(T)$:

$$\tau_s^{MKS}(\{\psi\}, T) = \frac{1}{2}\sum_{i=1}^{\infty} f_i(T)|\nabla\psi_i|^2. \quad (2)$$

The remaining term is the finite-T Thomas-Fermi KED [31],

$$\tau_{TF}(n, T) = t_{TF}(n)\xi(t), \quad (3)$$

where $t_{TF}(n) = 0.3(3\pi^2)^{2/3}n^{5/3}$, $\xi(t)$ is a combination of Fermi-Dirac integrals [32], and t is the reduced temperature, $T/T_F = 2/\beta[3\pi^2 n]^{2/3}$ with $\beta = (k_B T)^{-1}$. Both this term and the MKS T-dependent orbital KED reduce to their respective ground-state expressions, so $\lim_{T\to 0}\alpha_T(n, \nabla n, \{\psi\}) = \alpha(n, \nabla n, \{\psi\})$. In the high-temperature limit, the MKS kinetic energy approaches that of the HEG, τ_{TF}, such that with $t_{vW}(n, \nabla n) \to 0$, the isoorbital indicator naturally recovers metallic behavior $\alpha_T(n, \nabla n, \{\psi\}) \to 1$ expected for the HEG.

In addition to α_T, the XC free energy depends on the electron density and its gradient. We note that *f*TSCAN is developed under the assumption of non-spin-polarization, such that $\zeta = (n_\uparrow - n_\downarrow)/(n_\uparrow + n_\downarrow) = 0$. We can rely on LDA-level XC free energies and temperature-dependent density gradient variables developed in the course of earlier work on thermal LDA and GGA functionals [19–21]. The temperature-dependent reduced density gradients for exchange (s_{2x}) and correlation (q_c) are derived from the second-order gradient correction to the XC free energy and recover the ground state reduced density gradients s and $\mathcal{Q}$ (defined below) at $T = 0$ K. Detailed development is in Ref. [20]. Both are simple expressions comprised of the ground-state functional variable multiplied by a t-dependent factor for the former and a t- and density-dependent (via $r_s = (3/4\pi n)^{1/3}$) factor for the latter:

$$s_{2x}(n, \nabla n, T) = s^2(n, \nabla n)\frac{\widetilde{B}_x(t)}{\widetilde{A}_x(t)} \quad (4)$$

and

$$q_c(n, \nabla n, T) = \mathcal{Q}(n, \nabla n)\widetilde{B}_c(r_s, t). \quad (5)$$

Here, $\widetilde{B}_x(t)$, $\widetilde{A}_x(t)$, and $\widetilde{B}_c(r_s, t)$ are Padé approximants for Fermi-Dirac integral combinations [33]. The dimensionless variables are

$$s := \frac{|\nabla n(\mathbf{r})|}{2k_F n(\mathbf{r})}, \quad (6)$$

$$\mathcal{Q} := \frac{|\nabla n(\mathbf{r})|}{2k_s n(\mathbf{r})}, \quad (7)$$

with $k_F = (3\pi^2 n(\mathbf{r}))^{1/3}$ the Fermi wavevector and $k_s = \sqrt{4k_F/\pi}$.

Along with the LDA XC free energy density f_{xc}, the three T-dependent variables enable construction of the XC free energy density functional with full inclusion of thermal and inhomogeneity effects up through the meta-GGA level.

The SCAN ground-state exchange energy is given by

$$E_x[n] = \int d\mathbf{r} n(\mathbf{r})\varepsilon_x^{LDA}(n)F_x(s, \alpha), \quad (8)$$

where ε_x^{LDA} is the ground-state LDA exchange energy per particle and $F_x(s, \alpha)$ is the exchange enhancement factor. It

has the form

$$F_{\rm x}(s,\alpha) = h_{\rm x}^1(s,\alpha) + \theta(\alpha)\big[h_{\rm x}^0 - h_{\rm x}^1(s,\alpha)\big]g_{\rm x}(s), \quad (9)$$

where $\theta(\alpha)$ is an interpolation function governing the balance between the $h_{\rm x}^1$ (for $\alpha \approx 1$) and $h_{\rm x}^0 = 1.174$ contributions [5] and fulfilling the conjectured bound $F_{\rm x} \leqslant 1.174$ for all α [34]. In moving to a fully temperature-dependent functional, $\theta(\alpha)$ becomes a function of the T-dependent α_T variable.

The key term is $h_{\rm x}^1$, which in SCAN is given by

$$h_{\rm x,SCAN}^1 = 1 + \frac{k_{1\rm x}x}{k_{1\rm x}+x}, \quad (10)$$

with $k_{1\rm x} = 0.065$. This expression has the same form as the PBE exchange enhancement factor [7], for which $x = \mu s^2$. In SCAN, x is more complicated, with dependence on both s and α, which enables recovery of the fourth-order gradient expansion for exchange (see Supplemental Material [35] for detailed expressions). Thermal effects are accounted for by the use of T-dependent variables $s_{2\rm x}$ and α_T. But the presence of a sign change [20] in $s_{2\rm x}$ that has no counterpart in s^2 can cause numerical instability if $x \to -k_{1\rm x}$. To avoid that, we modify $h_{\rm x}^1$ slightly:

$$h_{\rm x,}{}_f{\rm TSCAN}^1 = 1 + \frac{k_{1\rm x}x}{k_{1\rm x}+|x|}. \quad (11)$$

The change is inspired by a similar manipulation [20] in the exchange enhancement factor of the KDT16 functional.

Finally, there is the matter of the factor $g_{\rm x}(s)$. We leave this factor unchanged in fTSCAN because of its $T = 0$ K form:

$$g_{\rm x}(s) = 1 - \exp\left[\frac{-a_1}{\sqrt{s}}\right]. \quad (12)$$

Since $s_{2\rm x}$ has a T-dependent sign change, simply replacing s with $s_{2\rm x}$ in Eq. (12) would introduce unphysical imaginary $g_{\rm x}$ values or a singularity as $s_{2\rm x} \to 0$. As $g_{\rm x}$ in SCAN enforces the vanishing of $F_{\rm x} \propto s^{-1/2}$ as $s \to \infty$, it is adequate to use that same quenching in fTSCAN, thereby avoiding the $s_{2\rm x}$ sign change problem.

The exchange free energy then is given by

$$\mathcal{F}_{\rm x}[n,T] = \int d\mathbf{r} n f_{\rm x}^{\rm LDA}(n,T) F_{\rm x}(s_{2\rm x},\alpha_T) \quad (13)$$

with the per-particle LDA exchange free energy presented in the factorized form [36] $f_{\rm x}^{\rm LDA}(n,T) = \varepsilon_{\rm x}^{\rm LDA}(n)\tilde{A}_{\rm x}(t)$, and $F_{\rm x}(s_{2\rm x},\alpha_T)$ the T-dependent exchange enhancement factor.

The fTSCAN correlation free energy is constructed in a similar fashion as the fTSCAN exchange free energy via replacement of ground-state functional variables with explicitly T-dependent reduced density gradients and isoorbital indicator. One ground-state ingredient that requires additional consideration is the so-called LSDA0 correlation energy, derived from the correlation energy of a two-electron system [37]. Unlike the HEG, for which accurate RPIMC XC free energies permit parametrization of a finite-temperature XC functional [17–19,21], the LSDA0 correlation energy must be tackled with a different strategy. Absent a parametrization of two-electron system thermal effects, we use a simple multiplicative scheme to approximate the T dependence. A T-dependent factor is determined from low-T ($T = 10^{-4}T_{\rm F}$, or $t = 10^{-4}$) and finite-T correlation energies by use of the corrKSDT thermal LDA functional, $f_{\rm c}^{\rm corrKSDT}(n,T) = f_{\rm xc}^{\rm corrKSDT}(n,T) - f_{\rm x}^{\rm LDA}(n,T)$, which is multiplied by the ground-state LSDA0 correlation energy:

$$f_{\rm c}^{\rm LDA0}(n,T) = \varepsilon_c^{\rm LDA0}(n)\frac{f_{\rm c}^{\rm corrKSDT}(n,T)}{f_{\rm c}^{\rm corrKSDT}(n,T=10^{-4}T_{\rm F})}. \quad (14)$$

The remainder of the correlation free energy is constructed straightforwardly in a manner analogous to the thermalization of the exchange free energy, with detailed expressions available in the Supplemental Material [35].

Performance testing. Benchmarking ground-state XC functional performance is a relatively mature process involving comparison with thermochemical data [38,39], molecular geometries [40,41], lattice constants and bulk moduli [24,42–44], and more [45,46]. Experimental data are abundant. The context for testing thermal XC functionals, especially in the challenging WDM regime, is rather more grim. Experimental data are sparse. The gold standard in computational accuracy under finite-T conditions is data from path-integral Monte Carlo (PIMC) calculations. Those, however, become prohibitively expensive at lower temperatures and less accurate due to the fermion sign problem. Worse, at temperatures for which PIMC data are accessible, the XC free energy often is negligible compared to the noninteracting free energy and the performance of various XC functionals becomes nearly identical.

To evaluate the performance of the fTSCAN functional, we start with static calculations on simple test systems, dense H and Al. All computational details are provided in the Supplemental Material [35] (including Refs. [47–50]). This allows us to compare the temperature evolution provided by the fTSCAN functional to that of other thermal and ground-state functionals. Then we provide a comparison to PIMC results on warm dense hydrogen. Finally, we consider more complex systems, confirming that (1) the thermalization process to construct fTSCAN has not disrupted the impressive accuracy of ground-state SCAN and (2) fTSCAN demonstrates improvements over ground-state functionals under finite-T conditions.

Warm dense hydrogen. Here, we examine finite-T XC effects at the meta-GGA level via static calculations on a simple cubic (sc) H model system with density $\rho = 0.6\,{\rm g/cm^3}$ (corresponding to $r_{\rm s} = 1.6$) and temperatures up to about $T = 35\,{\rm eV}$. Figure 1(a) shows the electronic pressure calculated using the KDT16, SCAN, and fTSCAN functionals as a relative difference to the electronic pressure from the ground-state GGA PBE functional.

At low T, there is a clear separation between GGA (PBE and KDT16) and meta-GGA (SCAN and fTSCAN) pressures. Small differences between ground-state and thermal functionals of the same refinement rung (e.g., PBE vs. KDT16, SCAN vs fTSCAN) at such temperatures arise from a small difference between ground-state LDA (PZ) and thermal LDA (corrKSDT) correlation energies [19].

As T goes above about 1 eV, differences between ground-state and thermal functionals (which highlight thermal effects) become more prominent than differences between GGA and meta-GGA functionals (which highlight inhomogeneity effects). For the ground-state approximation (GSA), the SCAN

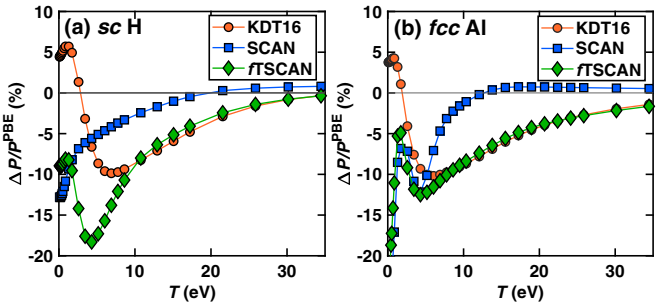

FIG. 1. Electronic pressure percentage differences relative to PBE values as a function of T calculated using the KDT16, SCAN, and fTSCAN functionals for (a) sc H at $\rho = 0.6\,\mathrm{g/cm^3}$ and (b) dense fcc Al at $\rho = 3.0\,\mathrm{g/cm^3}$.

electronic pressures converge fairly smoothly on the PBE data. However, electronic pressures calculated with thermal KDT16 and fTSCAN take a more complicated path. This indicates that inclusion of explicit T dependence has captured additional underlying behavior compared to the GSA in the warm dense matter temperature range. Note that at this density ($\rho = 0.6\,\mathrm{g/cm^3}$), the KDT16 and fTSCAN electronic pressures converge for temperatures above $T \approx 12\,\mathrm{eV}$ but have clear differences at lower temperatures. Finally, at very high T the electronic pressures from all the functionals—ground-state and thermal alike—converge. This convergence is due to the fact that in the high-T limit the noninteracting free-energy contribution dominates such that the XC contribution to the total free energy becomes negligible.

A recent survey [51] of simulations of warm dense hydrogen gave strong evidence for the importance of explicit thermal effects in XC functionals, with improved agreement with first-principles (FP) PIMC results from use of the thermal KDT16 rather than the ground-state PBE GGA functional. Tests of fTSCAN for selected r_s and temperature values show similar agreement with FP-PIMC data [52] as with KDT16 and improvement over PBE (summarized in Table I). For the lower densities explored ($r_s = 4$ or 8), the differences between GGA and meta-GGA are minor and even at lower temperatures KDT16 and fTSCAN results are very similar. At higher density, $r_s = 1.6$, some minor difference between KDT16 and fTSCAN manifests at lower temperatures. But they are once more nearly identical at the temperatures for which PIMC data are available. Nevertheless, the importance of T-dependent XC functionals is reinforced.

Dense aluminum. Static calculations on dense fcc Al ($\rho = 3.0\,\mathrm{g/cm^3}$) reveal a curious effect manifesting in the T dependence of the ground-state SCAN functional [Fig. 1(b)]. Differences in the behavior of the ground-state (PBE and SCAN) and thermal (KDT16 and fTSCAN) functionals of the same level of refinement demonstrate the change due to inclusion of temperature dependence at the GGA and meta-GGA levels. Differences in the behavior of two thermal or two ground-state functionals are the mark of inhomogeneity effects: the difference between KDT16 and fTSCAN contrasts between thermal effects at the GGA and meta-GGA levels.

As with the static calculations on sc H, there is a clear delineation between thermal and ground-state functionals starting from fairly low temperatures. For temperatures above about 7 eV, there is a very close correspondence between KDT16 and fTSCAN, marking the dominance of thermal effects over differences due to inhomogeneity. However, the calculations using SCAN follow a distinctive path, aligning below about 5 eV with the thermal functionals before eventually converging on the PBE results above roughly 15 eV.

Most plausibly, the source of this mixed alignment with thermal and ground-state functionals is the orbital kinetic energy. There is a subtlety in some implementations (including in the VASP package employed here) of ground-state meta-GGAs due to the explicit inclusion of Fermi-Dirac occupation numbers in the KS kinetic energy density. The ground-state approximation implementation for such a functional therefore actually relies on the MKS KED [see Eq. (2)], i.e., with explicit T dependence, along with the implicit T dependence in $n(\mathbf{r}, T)$.

Such a partial thermalization will be present for any ground-state orbital-dependent meta-GGA for which Fermi-Dirac occupations in the MKS kinetic energy are evaluated at the system electronic temperature, not $T = 0\,\mathrm{K}$. There are consequences to this. First, for $T \neq 0$, orbital-dependent meta-GGAs should be considered neither as purely ground state nor as fully thermal functionals. This incomplete thermalization is not the same for every meta-GGA, as the orbital kinetic energy is incorporated differently depending on the choice of isoorbital indicator and how that variable is used in the computation of XC energies. An important consequence is that correction schemes in which thermal effects from a lower-level functional are used

TABLE I. Comparison of total pressure data for warm dense hydrogen between PIMC reference data [52] and computed using the ground-state PBE (GGA) versus the free-energy KDT16 (GGA) and fTSCAN (meta-GGA) XC functionals. Relative differences are given in parentheses as percentages.

r_s	T (K)	P^{PIMC} (Mbar)	P^{PBE} (Mbar)	P^{KDT16} (Mbar)	$P^{f\mathrm{TSCAN}}$ (Mbar)
1.6	50000	N/A	4.53 (–)	4.45 (–)	4.33 (–)
1.6	125000	10.85	11.385 (4.9)	11.063 (1.9)	11.057 (1.9)
1.6	181825	16.59	17.069 (2.9)	16.709 (0.7)	16.729 (0.8)
4	15625	0.0452	0.0450 (-0.4)	0.0403 (-10.8)	0.0403 (-10.8)
4	31250	0.1158	0.1213 (4.8)	0.1130 (-2.4)	0.112 (-3.3)
4	62500	0.297	0.308 (3.7)	0.298 (0.34)	0.301 (1.4)
4	95250	0.52179	0.526 (0.8)	0.522 (0.1)	0.525 (0.6)
8	31250	0.0159			0.0163 (2.5)

to augment ground-state functionals [14,22,23] should not be applied to orbital-dependent meta-GGAs. One cannot account systematically for the thoroughness nor accuracy of temperature dependence in such a scheme [53].

In contrast, deorbitalized meta-GGAs depend on the density Laplacian rather than the orbital kinetic energy. Thus, they do not have this uncontrolled thermalization. One such recently developed functional is SCAN-L [54,55]. It has been adapted to include thermal effects at the GGA level through an additive correction strategy, resulting in the T-SCAN-L functional [14]. It has been used successfully in a variety of DFT explorations of warm dense matter, including calculations of the EOS of CHON resin [56] and deuterium [57], as well as examination of shock-induced polystyrene metallization [58]. The crucial distinction, however, is that *f*TSCAN represents a technical advance by explicit thermalization not simply at the GGA level but the full metaGGA level.

Water. The orbital dependence of conventional meta-GGA functionals can make them an especially fraught choice for the study of systems in which large numbers of bands are necessary either because of system size or thermal excitations. In that context, the absence of orbital dependence in deorbitalized exchange-correlation functionals such as SCAN-L therefore is appealing. An important challenge is that KED approximations used to deorbitalize some ground-state functional can be of limited accuracy in describing covalently bonded systems. Furthermore, their $T > 0$ generalizations are not well-studied.

Among these challenging systems is water, an admittedly complex substance involving multiple interatomic and intermolecular interactions of various strengths. Previous work had success in using SCAN to model both the structure and dynamics of water under ambient conditions [59]. We performed AIMD simulations on bulk water at 300 K to examine the effects of deorbitalization and thermalization, comparing four functionals: orbital-dependent ground-state SCAN and fully-thermal *f*TSCAN as well as deorbitalized ground-state SCAN-L and thermal (via additive correction) T-SCAN-L.

Differences are immediately apparent between the mean squared displacements (MSDs) of the oxygen and hydrogen atoms computed using the orbital-dependent and deorbitalized functionals [Figs. 2(a) and 2(b)], suggestive of very different dynamical behavior. The nearly flat MSD computed using deorbitalized functionals suggests artificial solidification of the system, while the roughly linearly increasing MSD computed with orbital-dependent functionals indicates proper liquid character. These differences appear for both the ground-state and thermal functionals, a clear indication that deorbitalization, not thermalization, is the cause. Furthermore, examination of the O-O pair distribution function, $g_{OO}(r)$, clearly shows significant deviations from experimental data [60] when using deorbitalized [Fig. 2(c)] functionals but excellent agreement with orbital-dependent functionals [Fig. 2(d)]. Since the deorbitalized functionals fail to capture the liquid character of water under these conditions, the resulting $g_{OO}(r)$ displays too-sharp and too-strong peaks, reflecting the incorrect retention of crystalline ordering.

At 300 K, thermal effects are expected to be negligible. Indeed, as with the MSD, the SCAN-L and T-SCAN-L $g_{OO}(r)$ are essentially identical, as are the SCAN and *f*TSCAN $g_{OO}(r)$. This confirms that thermalization has not disrupted the excellent performance of ground-state SCAN at low temperatures. As T increases, the relative importance of inhomogeneity effects—seen in the performance of meta-GGAs compared to lower-level functionals—will diminish as the importance of thermal effects comes to dominate the system. *f*TSCAN includes the best of both worlds, combining meta-GGA-level accuracy in handling inhomogeneity effects with full inclusion of thermal effects. Furthermore, although in this case orbital dependence appears to be necessary for accurate computations, deorbitalized meta-GGAs remain a plausible avenue for enabling DFT simulations at very high temperatures. Deorbitalization of *f*TSCAN will therefore be a topic of future investigations.

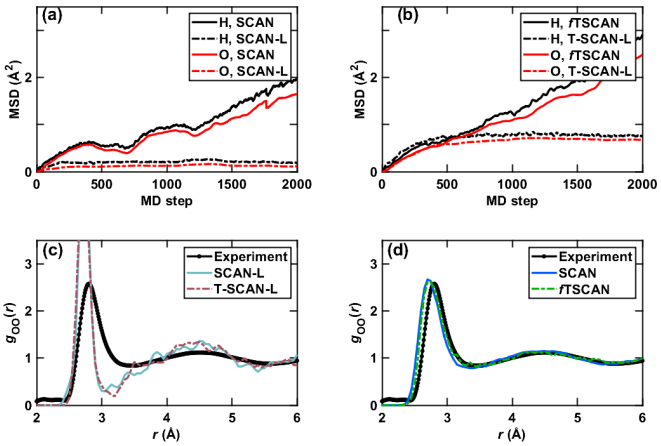

FIG. 2. Results of DFT-MD simulations of water at ambient conditions. (a), (b) Mean squared displacements (MSDs) for H (black) and O (red) calculated using SCAN, SCAN-L, *f*TSCAN, and T-SCAN-L. MSDs for deorbitalized functionals are plotted with dashed lines. Bottom: Comparison of pair distribution functions $g_{OO}(r)$ obtained from x-ray diffraction experiments (black) to computations using (c) orbital-free functionals SCAN-L (teal) and T-SCAN-L (brown) and (d) orbital-dependent functionals SCAN (blue) and *f*TSCAN (green).

Cold curve of stishovite SiO_2. Generation of material equations of state across broad temperature-density ranges necessitates accurate cold curves (usually requiring the use of meta-GGA functionals) and correct handling of thermal effects, both of which are readily achieved by the *f*TSCAN functional. The inclusion of XC effects through the meta-GGA level of refinement also improves the calculation of solid lattice constants [24,25]. It is well-known that LDA and GGA functionals tend to overbind and underbind, respectively, yielding generally too-small and too-large lattice constants. The PBEsol GGA functional [61] was developed specifically to improve the description of lattice constants for solids by using the correct second-order gradient coefficient for exchange.

Figure 3 compares the pressure-volume curve at 300 K for SiO_2 in the stishovite structure calculated with a variety of XC functionals with experimental values obtained from diamond anvil cell experiments [62–65]. Results from the meta-GGA functionals SCAN and *f*TSCAN, as well as the aforementioned GGA PBEsol, are in much closer agreement

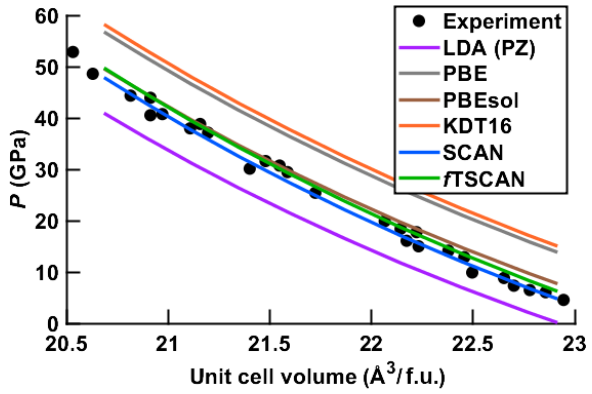

FIG. 3. Comparison of computed cold curves for SiO_2 in the stishovite structure for a variety of XC functionals with experimental data (black points). Meta-GGA functionals SCAN and fTSCAN, along with the GGA PBEsol functional greatly outperform the remaining GGA and LDA functionals.

with the experimental data than those calculated with the PBE or KDT16 GGA functionals, or the LDA (PZ) functional.

Conclusions. A fully-thermal meta-GGA free-energy XC functional fTSCAN, based on the ground-state SCAN (strongly constrained and appropriately normed) functional has been developed. Thermal effects are incorporated via T dependence in the ingredients: LDA free energies, reduced density gradients, and kinetic energy terms. Successful reproduction of the zero-T behavior of ground-state SCAN, a regime in which meta-GGA functionals typically are more accurate than lower-level functionals, is coupled with adherence to high-T limits where XC contributions become negligible. In the intermediate temperature range characteristic of the WDM regime, fTSCAN outperforms ground-state functionals and achieves similar levels of accuracy as the thermal GGA KDT16 functional while providing greater generality.

The thermalization scheme utilized in the construction of fTSCAN is readily transferable to regularized-restored [6] functionals and deorbitalized counterparts [66] derived from SCAN. Deorbitalization allows for vast improvements in computational scaling over orbital-based methods, advantageous for calculations in the WDM regime which require large numbers of bands. The regularization-restoration procedure follows from the troubling numerical behavior exhibited by SCAN in the high numbers of iterations required for convergence of an SCF loop and its extreme sensitivity to the density of numerical integration grids. The recent regularized and restored (r^{2}SCAN) functional [6] relaxes certain constraints for drastic improvements in computational stability. The accuracy of r^{2}SCAN remains on par with SCAN over several test sets [67]. Since numerical stability becomes increasingly important for computations requiring thousands of SCF iterations—such as AIMD simulations—adapting fTSCAN to the regularized-restored framework will be key.

Acknowledgments. We gratefully acknowledge J. D'Souza for helpful discussions regarding SiO_2 and for providing cold curve data for various XC functionals in Fig. 3. This material is based upon work supported by the Department of Energy (National Nuclear Security Administration) University of Rochester National Inertial Confinement Fusion Program under Award No. DE-NA0004144 as well as the U.S. National Science Foundation PHY Grant No. 2205521.

This report was prepared as an account of work sponsored by an agency of the U.S. Government. Neither the U.S. Government nor any agency thereof, nor any of their employees, makes any warranty, express or implied, or assumes any legal liability or responsibility for the accuracy, completeness, or usefulness of any information, apparatus, product, or process disclosed, or represents that its use would not infringe privately owned rights. Reference herein to any specific commercial product, process, or service by trade name, trademark, manufacturer, or otherwise does not necessarily constitute or imply its endorsement, recommendation, or favoring by the U.S. Government or any agency thereof. The views and opinions of authors expressed herein do not necessarily state or reflect those of the U.S. Government or any agency thereof.

Data availability. The data are available from the authors upon reasonable request.

[1] P. Hohenberg and W. Kohn, Inhomogeneous electron gas, Phys. Rev. **136**, B864 (1964).

[2] W. Kohn and L. J. Sham, Self-consistent equations including exchange and correlation effects, Phys. Rev. **140**, A1133 (1965).

[3] O. Gunnarsson and B. I. Lundqvist, Exchange and correlation in atoms, molecules, and solids by the spin-density-functional formalism, Phys. Rev. B **13**, 4274 (1976).

[4] D. C. Langreth and J. P. Perdew, Exchange-correlation energy of a metallic surface: Wave-vector analysis, Phys. Rev. B **15**, 2884 (1977).

[5] J. Sun, A. Ruzsinszky, and J. P. Perdew, Strongly constrained and appropriately normed semilocal density functional, Phys. Rev. Lett. **115**, 036402 (2015).

[6] J. W. Furness, A. D. Kaplan, J. Ning, J. P. Perdew, and J. Sun, Accurate and numerically efficient r^{2}SCAN meta-generalized gradient approximation, J. Phys. Chem. Lett. **11**, 8208 (2020).

[7] J. P. Perdew, K. Burke, and M. Ernzerhof, Generalized gradient approximation made simple, Phys. Rev. Lett. **77**, 3865 (1996). **78**, 1396(E) (1997).

[8] A. D. Kaplan, M. Levy, and J. P. Perdew, The predictive power of exact constraints and appropriate norms in density functional theory, Annu. Rev. Phys. Chem. **74**, 193 (2023).

[9] F. Graziani, M. P. Desjarlais, R. Redmer, and S. B. Trickey, *Frontiers and Challenges in Warm Dense Matter* (Springer Science & Business, Heidelberg, 2014), Vol. 96.

[10] S. X. Hu, V. N. Goncharov, T. R. Boehly, R. L. McCrory, S. Skupsky, L. A. Collins, J. D. Kress, and B. Militzer, Impact of first-principles properties of deuterium-tritium on inertial confinement fusion target designs, Phys. Plasmas **22**, 056304 (2015).

[11] S. X. Hu, L. A. Collins, T. R. Boehly, Y. H. Ding, P. B. Radha, V. N. Goncharov, V. V. Karasiev, G. W. Collins, S. P. Regan, and E. M. Campbell, A review on *ab initio* studies of static,

transport, and optical properties of polystyrene under extreme conditions for inertial confinement fusion applications, Phys. Plasmas **25**, 056306 (2015).
[12] N. D. Mermin, Thermal properties of the inhomogeneous electron gas, Phys. Rev. **137**, A1441 (1965).
[13] V. V. Karasiev, L. Calderín, and S. B. Trickey, Importance of finite-temperature exchange correlation for warm dense matter calculations, Phys. Rev. E **93**, 063207 (2016).
[14] V. V. Karasiev, D. I. Mihaylov, and S. X. Hu, Meta-GGA exchange-correlation free energy density functional to increase the accuracy of warm dense matter simulations, Phys. Rev. B **105**, L081109 (2022).
[15] V. V. Karasiev, S. X. Hu, M. Zaghoo, and T. R. Boehly, Exchange-correlation thermal effects in shocked deuterium: Softening the principal Hugoniot and thermophysical properties, Phys. Rev. B **99**, 214110 (2019).
[16] Z. Moldabekov, S. Schwalbe, M. P. Böhme, J. Vorberger, X. Shao, M. Pavanello, F. R. Graziani, and T. Dornheim, Bound-state breaking and the importance of thermal exchange-correlation effects in warm dense hydrogen, J. Chem. Theory Comput. **20**, 68 (2024).
[17] E. W. Brown, B. K. Clark, J. L. DuBois, and D. M. Ceperley, Path-integral Monte Carlo simulation of the warm dense homogeneous electron gas, Phys. Rev. Lett. **110**, 146405 (2013).
[18] T. Dornheim, S. Groth, T. Sjostrom, F. D. Malone, W. M. C. Foulkes, and M. Bonitz, *Ab initio* quantum Monte Carlo simulation of the warm dense electron gas in the thermodynamic limit, Phys. Rev. Lett. **117**, 156403 (2016).
[19] V. V. Karasiev, T. Sjostrom, J. Dufty, and S. B. Trickey, Accurate homogeneous electron gas exchange-correlation free energy for local spin-density calculations, Phys. Rev. Lett. **112**, 076403 (2014).
[20] V. V. Karasiev, J. W. Dufty, and S. B. Trickey, Nonempirical semilocal free-energy density functional for matter under extreme conditions, Phys. Rev. Lett. **120**, 076401 (2018).
[21] S. Groth, T. Dornheim, T. Sjostrom, F. D. Malone, W. M. C. Foulkes, and M. Bonitz, *Ab initio* exchange-correlation free energy of the uniform electron gas at warm dense matter conditions, Phys. Rev. Lett. **119**, 135001 (2017).
[22] T. Sjostrom and J. Daligault, Gradient corrections to the exchange-correlation free energy, Phys. Rev. B **90**, 155109 (2014).
[23] J. Kozlowski, D. Perchak, and K. Burke, Generalized gradient approximation made thermal, arXiv:2308.03319v2.
[24] F. Tran, J. Stelzl, and P. Blaha, Rungs 1 to 4 of DFT Jacob's ladder: Extensive test on the lattice constant, bulk modulus, and cohesive energy of solids, J. Chem. Phys. **144**, 204120 (2016).
[25] E. B. Isaacs and C. Wolverton, Performance of the strongly constrained and appropriately normed density functional for solid-state materials, Phys. Rev. Mater. **2**, 063801 (2018).
[26] J. Sun, B. Xiao, Y. Fang, R. Haunschild, P. Hao, A. Ruzsinszky, G. I. Csonka, G. E. Scuseria, and J. P. Perdew, Density functionals that recognize covalent, metallic, and weak bonds, Phys. Rev. Lett. **111**, 106401 (2013).
[27] J. W. Furness and J. Sun, Enhancing the efficiency of density functionals with an improved iso-orbital indicator, Phys. Rev. B **99**, 041119(R) (2019).
[28] M. Levy and Hui Ou-Yang, Exact properties of the Pauli potential for the square root of the electron density and the kinetic energy functional, Phys. Rev. A **38**, 625 (1988).
[29] J. W. Dufty and S. B. Trickey, Scaling, bounds, and inequalities for the noninteracting density functionals at finite temperature, Phys. Rev. B **84**, 125118 (2011).
[30] R. M. N. Goshadze, V. V. Karasiev, K. P. Hilleke, and S. X. Hu, On the Pauli potential formalism at finite temperature (unpublished).
[31] R. P. Feynman, N. Metropolis, and E. Teller, Equations of state of elements based on the generalized Fermi-Thomas theory, Phys. Rev. **75**, 1561 (1949).
[32] V. V. Karasiev, T. Sjostrom, and S. B. Trickey, Generalized-gradient-approximation noninteracting free-energy functionals for orbital-free density functional calculations, Phys. Rev. B **86**, 115101 (2012).
[33] V. V. Karasiev, D. Chakraborty, and S. B. Trickey, Improved analytical representation of combinations of Fermi-Dirac integrals for finite-temperature density functional calculations, Comput. Phys. Commun. **192**, 114 (2015).
[34] J. P. Perdew, A. Ruzsinszky, J. Sun, and K. Burke, Gedanken densities and exact constraints in density functional theory, J. Chem. Phys. **140**, 18A533 (2014).
[35] See Supplemental Material at http://link.aps.org/supplemental/10.1103/PhysRevMaterials.9.L050801 for a complete set of expressions for constructing *f*TSCAN exchange and correlation free-energies, computational details, and tabulated data for all figures.
[36] F. Perrot, Gradient correction to the statistical electronic free energy at nonzero temperatures: Application to equation-of-state calculations, Phys. Rev. A **20**, 586 (1979).
[37] J. Sun, J. P. Perdew, Z. Yang, and H. Peng, Communication: Near-locality of exchange and correlation density functionals for 1- and 2-electron systems, J. Chem. Phys. **144**, 191101 (2016).
[38] A. Karton, N. Sylvetsky, and J. M. L. Martin, W4-17: A diverse and high-confidence dataset of atomization energies for benchmarking high-level electronic structure methods, J. Comput. Chem. **38**, 2063 (2017).
[39] L. Goerigk, A. Hansen, C. Bauer, S. Ehrlich, A. Najibi, and S. Grimme, A look at the density functional theory zoo with the advanced GMTKN55 database for general main group thermochemistry, kinetics, and noncovalent interactions, Phys. Chem. Chem. Phys. **19**, 32184 (2017).
[40] É. Brémond, M. Savarese, N. Q. Su, Á. J. Pérez-Jiménez, X. Xu, J. C. Sancho-García, and C. Adamo, Benchmarking density functionals on structural parameters of small-/medium-sized organic molecules, J. Chem. Theory Comput. **12**, 459 (2016).
[41] O. A. Vydrov and T. Van Voorhis, Benchmark assessment of the accuracy of several van der Waals density functionals, J. Chem. Theory Comput. **8**, 1929 (2012).
[42] L. Schimka, R. Gaudoin, J. Klimeš, M. Marsman, and G. Kresse, Lattice constants and cohesive energies of alkali, alkaline-earth, and transition metals: Random phase approximation and density functional theory results, Phys. Rev. B **87**, 214102 (2013).
[43] K. Lejaeghere, V. van Speybroeck, G. Van Oost, and S. Cottenier, Error estimates for solid-state density functional theory predictions: An overview by means of the ground-state elemental crystals, Crit. Rev. Solid State Mater. Sci. **39**, 1 (2013).
[44] P. Janthon, S. Luo, S. M. Kozlov, F. Viñes, J. Limtrakul, D. G. Truhlar, and F. Illas, Bulk properties of transition metals:

A challenge for the design of universal density functionals, J. Chem. Theory Comput. **10**, 3832 (2014).

[45] M. Korth and S. Grimme, Mindless DFT benchmarking, J. Chem. Theory Comput. **5**, 993 (2009).

[46] P. Borlido, T. Aull, A. W. Huran, F. Tran, M. A. L. Marques, and S. Botti, Large-scale benchmark of exchange-correlation functionals for the determination of electronic band gaps of solids, J. Chem. Theory Comput. **15**, 5069 (2019).

[47] A. Baldereschi, Mean-value point in the Brillouin zone, Phys. Rev. B **7**, 5212 (1973).

[48] G. Kresse and J. Furthmüller, Efficient iterative schemes for *ab initio* total-energy calculations using a plane-wave basis set, Phys. Rev. B **54**, 11169 (1996).

[49] G. Kresse and J. Furthmüller, Efficiency of *ab-initio* total energy calculations for metals and semiconductors using a plane-wave basis set, Comput. Mater. Sci. **6**, 15 (1996).

[50] G. Kresse and D. Joubert, From ultrasoft pseudopotentials to the projector augmented-wave method, Phys. Rev. B **59**, 1758 (1999).

[51] M. Bonitz, J. Vorberger, M. Bethkenhagen, M. Böhme, D. Ceperley, A. Filinov, T. Gawne, F. Graziani, G. Gregori, P. Hamann, S. Hansen, M. Holzmann, S. X. Hu, H. Kählert, V. Karasiev, U. Kleinschmidt, L. Kordts, C. Makait, B. Militzer, Z. Moldabekov *et al.*, Towards first principles-based simulations of dense hydrogen, Phys. Plasmas **31**, 110501 (2024).

[52] A. V. Filinov and M. Bonitz, Equation of state of partially ionized hydrogen and deuterium plasma revisited, Phys. Rev. E **108**, 055212 (2023).

[53] V. V. Karasiev, K. P. Hilleke, and S. B. Trickey, Free-energy orbital-free density functional theory: Recent developments, perspective, and outlook, Electron. Struct. **7**, 013001 (2025).

[54] D. Mejia-Rodriguez and S. B. Trickey, Deorbitalization strategies for meta-generalized-gradient-approximation exchange-correlation functionals, Phys. Rev. A **96**, 052512 (2017); Erratum: Deorbitalization strategies for meta-generalized-gradient-approximation exchange-correlation functionals [Phys. Rev. A 96, 052512 (2017)], **111**, 029901(E) (2025).

[55] D. Mejía-Rodríguez and S. B. Trickey, Deorbitalized meta-GGA exchange-correlation functionals in solids, Phys. Rev. B **98**, 115161 (2018).

[56] S. Zhang, V. V. Karasiev, N. Shaffer, D. I. Mihaylov, K. Nichols, R. Paul, R. M. N. Goshadze, M. Ghosh, J. Hinz, R. Epstein, S. Goedecker, and S. X. Hu, First-principles equation of state of CHON resin for inertial confinement fusion applications, Phys. Rev. E **106**, 045207 (2022).

[57] D. I. Mihaylov, V. V. Karasiev, S. X. Hu, J. R. Rygg, V. N. Goncharov, and G. W. Collins, Improved first-principles equation-of-state table of deuterium for high-energy-density applications, Phys. Rev. B **104**, 144104 (2021).

[58] R. M. N. Goshadze, V. V. Karasiev, D. I. Mihaylov, and S. X. Hu, Shock-induced metallization of polystyrene along the principal Hugoniot investigated by advanced density functionals, Phys. Rev. B **107**, 155116 (2023).

[59] M. Chen, H.-Y. Ko, R. C. Remsing, M. F. Calegari Andrade, B. Santra, Z. Sun, A. Selloni, R. Car, M. L. Klein, J. P. Perdew, and X. Wu, *Ab initio* theory and modeling of water, Proc. Natl. Acad. Sci. USA **114**, 10846 (2017).

[60] L. B. Skinner, C. Huang, D. Schlesinger, L. G. M. Pettersson, A. Nilsson, and C. J. Benmore, Benchmark oxygen-oxygen pair-distribution function of ambient water from x-ray diffraction measurements with a wide Q-range, J. Chem. Phys **138**, 074506 (2013).

[61] J. P. Perdew, A. Ruzsinszky, G. I. Csonka, O. A. Vydrov, G. E. Scuseria, L. A. Constantin, X. Zhou, and K. Burke, Restoring the density-gradient expansion for exchange in solids and surfaces, Phys. Rev. Lett. **100**, 136406 (2008).

[62] D. Andrault, R. J. Angel, J. L. Mosenfelder, and T. Le Bihan, Equation of state of stishovite to lower mantle pressures, Am. Mineral. **88**, 301 (2003).

[63] R. J. Hemley, J. Shu, M. A. Carpenter, J. Hu, H. K. Mao, and K. J. Kingma, Strain/order parameter coupling in the ferroelastic transition in dense SiO_2, Solid State Commun. **114**, 527 (2000).

[64] N. L. Ross, J.-F. Shu, and R. M. Hazen, High-pressure crystal chemistry of stishovite, Am. Min. **75**, 739 (1990).

[65] R. A. Fischer, A. J. Campbell, B. A. Chidester, D. M. Reaman, E. C. Thompson, J. S. Pigott, V. B. Prakapenka, and J. S. Smith, Equations of state and phase boundary for stishovite and $CaCl_2$-type SiO_2, Am. Min. **103**, 792 (2018).

[66] D. Mejía-Rodríguez and S. B. Trickey, Meta-GGA performance in solids at almost GGA cost, Phys. Rev. B **102**, 121109(R) (2020).

[67] R. Kingsbury, A. S. Gupta, C. J. Bartel, J. M. Munro, S. Dwaraknath, M. Horton, and K. A. Persson, Performance comparison of r^2SCAN and SCAN metaGGA density functionals for solid materials via an automated, high-throughput computational workflow, Phys. Rev. Mater. **6**, 013801 (2022).